Available online at www.sciencedirect.com
SCIENCE DIRECT®
Fluid Phase Equilibria 233 (2005) 204–219
FLUID PHASE EQUILIBRIA
www.elsevier.com/locate/fluid

Multiparameter crossover equation of state: Generalized algorithm and application to carbon dioxide

Lixin Sun, Sergei B. Kiselev, James F. Ely *

Department of Chemical Engineering, Colorado School of Mines, Golden, CO 80401, USA

Received 27 July 2004; received in revised form 26 April 2005; accepted 26 April 2005

Abstract

In this work, we propose a new optimization algorithm for the development of multiparameter crossover equations of state (MC EOS), which incorporates the asymptotic scaling laws near the critical point. This algorithm is based on stepwise regression, which reduces the intercorrelations among the functional terms in the equation and enables the incorporation of the universal crossover formulation into the development of equations of state. The EOS developed is optimized in structure and gives correct prediction of caloric properties in the immediate vicinity of the critical point. For the determination of the linear, analytical coefficients and the non-linear crossover parameters in the crossover EOS for a given fluid, both linear and non-linear optimization procedures are used. By applying this algorithm we have developed a wide-range crossover equation of state (EOS) for carbon dioxide in the form of dimensionless Helmholtz energy. The derived MC EOS contains only 26 functional terms, and gives excellent descriptions of experimental data over a wide-range of states. Compared to the extremely accurate standard reference equation of state of Span and Wagner (SW EOS), the MC EOS yields a very good description of thermodynamic surfaces away from the critical point. In one-phase region, the MC EOS represents the experimental values of density with an average absolute deviation (AAD) of about 0.1%, and pressure with an AAD of about 0.3%. However, unlike the SW EOS, the MC EOS reproduces the well-established scaling laws behavior in the asymptotic critical region as $T \rightarrow T_c$.

Keywords: Carbon dioxide; Crossover theory; Equation of state; Optimization algorithm; Pure fluids; Thermodynamic properties

1. Introduction

During the last two decades great progress has been achieved in the development of highly accurate empirical multiparameter equations of state (EOS) for pure fluids [1,2]. This became possible not only because of significant improvements in thermodynamic measurment techniques [3], but also because of the evolution of algorithms for the optimization of the structure of multiparameter thermodynamic equations of state. Wagner [4] in 1974 applied a stepwise (STW) regression analysis for the development of an equation for vapor pressure, and then de Rueck and Armstrong [5] adopted this method to develop a wide-range EOS for propylene in 1979. Their work signaled the beginning of the development of EOS structure optimization algorithms, and has led to a series of new optimization algorithms in the following years. It was shown in later work that the structure optimized equations have higher accuracy compared to the equations developed with trial and error methods, and have drastically improved the numerical stability. This advantage clearly cannot be compensated for by simply increasing the number of terms in the equation [6].

Setzmann and Wagner [7] proposed an algorithm, OPTIM, based on a combination of stepwise regression and the evolutionary optimization method (EOM) in 1989 [8] and published its application to methane in 1991 [9]. This newer algorithm is relatively easy to start, and enables one to find a global optimum instead of a local optimum. Later, an algorithm combining stepwise regression and simulated annealing (SA) was proposed by Shubert and Ely to develop reference equations of state for R134a and R123 [10,11]. However,

* Corresponding author. Tel.: +1 303 273 3720; fax: +1 303 273 3730.
E-mail address: jely@mines.edu (J.F. Ely).

0378-3812/$ – see front matter © 2005 Elsevier B.V. All rights reserved.
doi:10.1016/j.fluid.2005.04.019

these linear regression algorithms could not directly use isobaric heat capacity and speed of sound data, because of their non-linearity respect to the adjustable parameters. Any "linearization" of these thermodynamic properties leads to potential loss of important experimental information. Optimization procedures based on the combination of linear and non-linear regression analysis, aimed to extend the regression to the non-linear properties, were proposed by Ahrendts and Baehr [12,13]. Recently, Tegeler et al. [14] proposed a non-linear optimization algorithm based on the OPTIM algorithm, and used a non-linear quality criterion for all relevant decisions. The algorithm is only a quasi-non-linear algorithm since it still depends on linear selection as the starting point. Using these algorithms, highly accurate reference equations of state for substances such as methane [9], carbon dioxide [15], water [16], argon [14], nitrogen [17] and ethylene [18] have been developed in the last decade. In addition, a large number of the moderately accurate, engineering quality, reference EOS has also been developed (for reviews see Refs. [1,2,19]).

In spite of the advances made in equation of state methodology, the resulting multiparameter equations are typically complicated in their structures; there are usually between 30 and 60 functional terms present in these equations. More importantly, these analytical–classical equations in principle cannot reproduce the non-analytical, singular behavior of the thermodynamic surface of pure fluids in the critical region. To overcome this shortcoming, some non-analytical terms have been added into recent state-of-the-art EOS [15,16] to improve the prediction of the isochoric heat capacity and speed of sound data in the critical region. Even though the modified state-of-the-art EOS describe all measured properties in the critical region [2,3], they still do not reproduce the theoretically well-established asymptotic scaling laws in this region [20,21]. Moreover, they give incorrect behavior of the specific heat and the speed of sound in the one-phase region and along the coexistence curve in the immediate vicinity of the critical point [15,22]. This behavior occurs strictly outside the range of available experimental data, but these shortcomings make the state-of-the-art EOS less attractive as scientific formulations for which they were developed.

A general procedure for transforming any classical equation of state into a crossover EOS, which reproduces the scaling laws in the asymptotic critical region and is transformed into the original classical EOS far away from the critical point, was proposed by Kiselev [23]. The procedure is based on renormalization-group theory and has been successfully applied to the cubic [23–25], SAFT [26–29] and semi-empirical square-well EOS [30]. A restricted revision of the state-of-the-art EOS for water was also proposed by Kiselev and Friend [22]. In this paper, we incorporate Kiselev's renormalization procedure [23] into the STW regression algorithm, thereby producing a structure-optimized equation that has a crossover form. We refer to this procedure as the generalized stepwise regression (GSTW). In this work, we have applied the GSTW regression algorithm to develop a highly accurate, while relatively compact multiparameter crossover equation of state (MC EOS) for carbon dioxide.

We proceed as follows. In Section 2, we consider the theoretical background for the crossover procedure of incorporating the scaling laws into a classical equation of state. In Section 3, we describe the GSTW algorithm for developing of a wide-range multiparameter crossover equation of state. The new MC EOS for carbon dioxide and its comparison with the state-of-the-art EOS of Span and Wagner [15] are given in Section 4. Our conclusions are summarized in Section 5.

2. Crossover Helmholtz energy model

Traditionally, engineering equations of state express the pressure in terms of the temperature and density. There are, however, functionalities in this pressure explicit form, which cannot be integrated analytically to obtain the desired thermodynamic properties. Because of this, modern multiparameter equations of state are represented in terms of the Helmholtz energy A as a function of temperature and density. Using this formulation, all thermodynamic properties can be represented by appropriate derivatives of the Helmholtz function.The dimensionless Helmholtz energy $\Phi(\delta, t) = A(\rho, T)/RT$ can be described as a linear combination of the ideal gas, $\Phi^{\mathrm{id}}(\delta, t)$, and residual, $\Phi^{\mathrm{r}}(\delta, t)$ contributions:

$$\Phi(\delta, t) = \Phi^{\mathrm{id}}(\delta, t) + \Phi^{\mathrm{r}}(\delta, t) = \Phi_0(t) + \ln(\delta) + \Phi^{\mathrm{r}}(\delta, t) \tag{1}$$

where $A(\rho, T)$ is the Helmholtz energy as a function of density, ρ, and temperature, T, R the gas constant, the reduced density and temperature are $\delta = \rho/\rho_{\mathrm{c}}$ and $t = T_{\mathrm{c}}/T$, respectively, and $\Phi_0(t)$ is the temperature dependent part of the ideal-gas contribution. The ideal part of Helmholtz energy is determined from experimental or theoretical knowledge of the ideal gas heat capacity. The empirical residual part of the Helmholtz energy is usually expressed as a linear combination of dimensionless density and temperature terms (so-called "functional terms") as shown in Eq. (2):

$$\begin{aligned}\Phi^{\mathrm{r}}(\delta, t) = {} & \sum_{m=1}^{M_1} a_m \delta^{i_m} t^{j_m} + \sum_{m=M_1+1}^{M_2} a_m \delta^{i_m} t^{j_m} \exp(-{}_m\delta^{k_m}) \\ & + \sum_{m=M_2+1}^{M_3} a_m \delta^{i_m} t^{j_m} \exp[-\alpha_m(\delta - \in_m)^2 \\ & - \beta_m(t - \gamma_m)^2]\end{aligned} \tag{2}$$

where a_m are the coefficients for each term, i_m, j_m and k_m exponents on t, δ and exponential δ terms, respectively, α_m, β_m, $\in_m$ and γ_m the parameters and M_1, M_2 and M_3 are the numbers of different type of terms. As can be seen from this equation, there are three types of terms—polynomial, exponential and Gaussian, viz., $\Phi^{\mathrm{r}} = \Phi^{\mathrm{r}}_{\mathrm{Pol}} + \Phi^{\mathrm{r}}_{\mathrm{Exp}} + \Phi^{\mathrm{r}}_{\mathrm{GS}}$. Expressions for the thermodynamic properties in terms of Eq.

(2) are given in Table A.1 in Appendix A and the required derivatives for the polynomial, exponential and Gaussian terms are given in Tables A.2 and A.3 in Appendix A. The parameters M_1, M_2, M_3, i_m, j_m and k_m for an analytical EOS result from the STW structure optimization, and the coefficients a_m in Eq. (2) for the residual part of the dimensionless Helmholtz energy (1) result from a linear, or non-linear, fit to experimental data. The critical parameters T_c and ρ_c, and the compressibility factor $Z_c = P_c/\rho_c RT_c$ of the Helmholtz model can be found from the conditions:

$$Z_c = \left(\frac{\partial\Phi}{\partial\delta}\right)_{T=T_c}, \qquad \left(\frac{\partial^2\Phi}{\partial\delta^2}\right)_{T=T_c} = 0,$$
$$\left(\frac{\partial^3\Phi}{\partial\delta^3}\right)_{T=T_c} = 0 \tag{3}$$

which are usually used as the critical-point constraints in the optimization algorithm.

A general procedure based on the fundamental results of the renormalization-group theory for transforming any classical equation of state into the crossover form was developed by Kiselev [23]. Following this procedure, one needs first to rewrite the classical expression Eq. (1) for the reduced Helmholtz energy in the form:

$$\Phi(\delta, t) = \Delta\Phi(\eta, \tau) - \eta p_0(t) + \Phi_0^r(t) + \Phi_0(t) \tag{4}$$

where the critical, or singular part of the Helmholtz energy, $\Delta\Phi(\eta, \tau)$, is a function of the order parameter $\eta = \delta^{-1} - 1 = \rho_c/\rho - 1$ and the dimensionless temperature deviation $\tau = t^{-1} - 1 = T/T_c - 1$. $p_0(t) = p(T, \rho_c)/\rho_c RT$ and $\Phi_0^r(t) = \Phi^r(1, t) = A^r(\rho_c, T)/RT$ are the dimensionless pressure and residual part of the Helmholtz energy along the critical isochore, $\rho = \rho_c$. The critical part of the dimensionless Helmholtz energy can be derived from Eqs. (1) and (4) as:

$$\Delta\Phi(\eta, \tau) = \Phi^r(\eta, \tau) - \Phi_0^r(\tau) - \ln(\eta + 1) + \eta p_0(\tau) \tag{5}$$

thereby satisfying the critical point conditions [31]:

$$\Delta\Phi(\eta = 0, \tau = 0) = 0, \qquad \left(\frac{\partial\Delta\Phi}{\partial\eta}\right)_{\eta=0,\tau=0} = 0,$$
$$\left(\frac{\partial^2\Delta\Phi}{\partial\eta^2}\right)_{\eta=0,\tau=0} = 0 \tag{6}$$

Secondly, one needs to replace τ and η in the critical part of the classical Helmholtz energy, $\Delta\Phi(\eta,\tau)$, by the renormalized values [32]:

$$\bar{\tau} = \tau Y^{-(\alpha/2\Delta_1)}, \qquad \bar{\eta} = \eta Y^{-(\gamma-2\beta)/4\Delta_1} \tag{7}$$

where

$$\alpha = 0.110, \quad \beta = 0.325, \quad \gamma = 2 - \alpha - 2\beta = 1.24,$$
$$\Delta_1 = 0.51 \tag{8}$$

are the universal critical exponents and Y is a crossover function to be specified below. Since in multiparameter equations of state, the critical parameters can always be set equal to the experimental values, Eq. (7) does not contain the critical shift terms introduced by Kiselev et al. for simpler cubic equations [23–25]. This simplification makes the crossover function Y formally independent of the analytical residual part Φ^r and allows us to use the linear regression for the optimization of Φ^r.

In order to complete transformation, one needs to add in Eq. (4) the so-called kernel term:

$$K(\tau) = \frac{1}{2}a_{20}\tau^2(Y^{-(\alpha/\Delta_1)} - 1) \tag{9}$$

which provides the correct scaling behavior of the specific isochoric heat capacity along the critical isochore asymptotically close to the critical point. The crossover function Y in Eqs. (7) and (9) can be written in parametric form [30]:

$$Y(q) = \left[\frac{q}{1 + (q^2/(1+q))}\right]^{\Delta_1} \tag{10}$$

where the parametric variable q is related to the order parameter η and the dimensionless temperature τ though equation [30]:

$$\frac{1}{b^2}\left(q^2 - \frac{\tau}{Gi}\right)\left[1 - \frac{1}{4}\left(1 - \frac{\tau}{q^2 Gi}\right)\right]$$
$$= \left[\frac{\eta + v_1\eta^3\,\exp(-\delta_1\eta) + d_1\tau(1-\tau)}{m_0 Gi^\beta}\right]^2 Y(q)^{(1-2\beta)/\Delta_1} \tag{11}$$

where Gi is the Ginzburg number of fluid of interest, $b^2 = 1.359$ a universal linear-model parameter, the parameter $\delta_1 = 8.5$ [24], and m_0, d_1 and v_1 are the system-dependent parameters. Eq. (11) must be solved at every thermodynamic state point since the model is continuous and smooth over the entire surface. Finally, the crossover expression for the Helmholtz energy can be rewritten in the form:

$$\Phi(\delta, t) = \Phi^{id}(\delta, t) + \hat{\Phi}^r(\delta, t) = \ln(\delta) + \Phi_0(t) + \hat{\Phi}^r(\delta, t) \tag{12}$$

where the renormalized residual part is given by:

$$\hat{\Phi}^r(\delta, t) = \Phi^r(\bar{\eta}, \bar{\tau}) - \Phi_0^r(\bar{\tau}) + \Phi_0^r(t) + \bar{\eta}p_0(\bar{\tau}) - \eta p_0(t) - \ln(\bar{\eta} + 1) + \ln(\eta + 1) - K(\tau) \tag{13}$$

Eqs. (7)–(13) completely determine the crossover Helmholtz energy for an arbitrary classical formulation $\Phi^r(\delta, t)$. Asymptotically close to the critical point $q \ll 1$ (or $|\tau| \ll Gi$ at the coexistence curve and along the critical isochore $\rho = \rho_c$) the crossover function $Y(q) \approx q^{\Delta_1}$, the renormalized parameters $\bar{\tau} \cong \tau q^{-(\alpha/2)}$ (or $\bar{\tau} \approx \tau^{(2-\alpha)/2}$ at $\rho = \rho_c$) and $\bar{\eta} \cong \eta q^{(\gamma-4\beta)/4}$ (or $|\bar{\eta}| \approx |\eta|^{(2-\alpha)/4\beta}$ at $T = T_c$) and the residual Helmholtz function $\hat{\Phi}^r(\delta, t)$ becomes a non-analytic function of τ and η, which after differentiation reproduces the theoretical scaling laws for the coexistence curve [20,21]:

$$\Delta\eta_{cxs} \simeq \pm B_0|\tau|^\beta(1 + B_1|\tau|^{\Delta_1}) \tag{14}$$

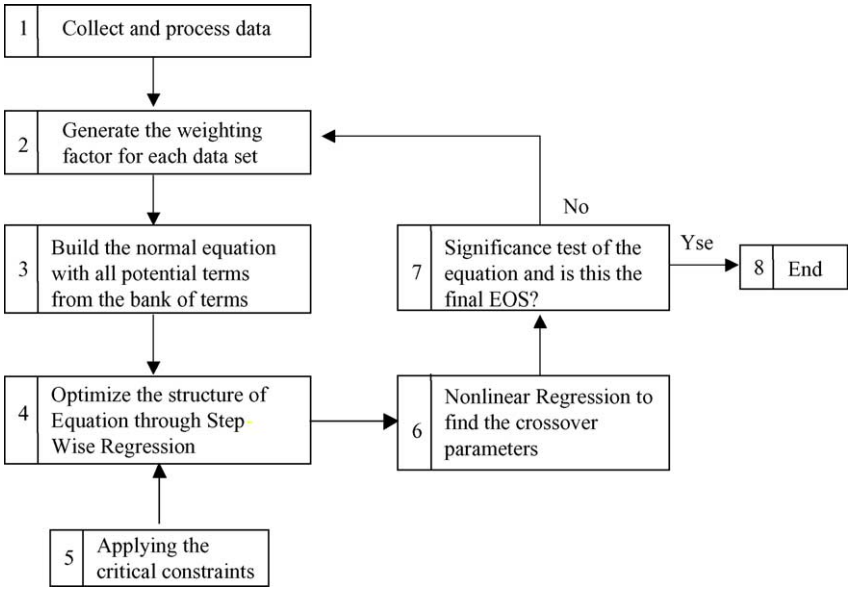

Fig. 1. Flowchart of the GSTW algorithm to develop multiparameter crossover equation of state.

where signs '±' correspond to the liquid (+) and vapor (−) phases, respectively. For the isothermal compressibility and the isochoric heat capacity we find:

$$\kappa_T = \frac{1}{\rho}\left(\frac{\partial\rho}{\partial p}\right)_T \simeq \Gamma_0^{\pm}|\tau|^{-\gamma}(1+\Gamma_1|\tau|^{\Delta_1}) \tag{15}$$

$$C_V = T\left(\frac{\partial S}{\partial T}\right)_\rho \simeq A_0^{\pm}|\tau|^{-\alpha}(1+A_1|\tau|^{\Delta_1}) + C_0 \tag{16}$$

where superscripts '±' in Eqs. (15) and (16) correspond to the supercritical ($T > T_c$) and subcritical ($T < T_c$) temperature regions, respectively. Far away from the critical point $q \gg 1$ (or $|\tau| \gg Gi$ at the coexistence curve and along the critical isochore $\rho = \rho_c$) the crossover function $Y(q) \cong 1$, the renormalized temperature and order parameter tend to their classical values $\bar{\tau} \to \tau$ and $\bar{\eta} \to \eta$, and the renormalized residual part is transformed into its classical analog $\hat{\Phi}^r(\delta, t) \to \Phi^r(\delta, t)$, and all thermodynamic properties exhibit an analytical–classical behavior as determined by Eq. (1).

Since Eq. (12) is a fundamental thermodynamic equation, all thermodynamic properties can be directly calculated from it by differentiation. The differential property relationships and the required derivatives of $\hat{\Phi}^r(\delta, t)$ with respect to δ and t are given in Tables A.4 and A.5 in Appendix A.

3. Optimization algorithm

The multiparameter crossover Helmholtz energy model defined by Eqs. (12) and (13) contains the following system-dependent parameters: classical parameters $a_m, i_m, j_m, k_m, \alpha_m, \beta_m, \varepsilon_m$ and γ_m in Eq. (1), the amplitude a_{20} of the kernel term $K(\tau)$ in Eq. (9), the Ginzburg number Gi and the crossover parameters m_0, v_1 and d_1 in Eq. (11). All these parameters and the final structure of the crossover Helmholtz energy can be found from the GSTW optimization algorithm shown in Fig. 1.

According to this algorithm, we first generate the weight for each data point with a known EOS, which is used as a starting input EOS for regression. We then build the regression matrix based on the linear least squares regression method, by converting the experimental data sets to their corresponding forms in the Helmholtz model with all the potential functional terms included into the term-bank. In the third step, we set the Ginzburg number $Gi = 0$ in Eq. (11), which is equivalent the condition $\Phi^r \equiv \hat{\Phi}^r$ in Eq. (12), and use the STW regression procedure proposed by de Reuck and Armstrong [5] to optimize the structure of the classical Helmholtz free-energy and the linear coefficients a_m and exponents i_m, j_m and k_m in Eq. (1). The critical constraints (6) are added into the STW by the method of Lagrangian multipliers [33] to ensure the resulting EOS has the correct critical parameters. In these steps, we use only linear data ($P\rho T$, $C_V(\rho, T)$, $(\partial p/\partial\rho)_T$, second virial coefficient and the coexistence curve) where the coexistence data were included into the STW regression through the Maxwell rules:

$$\frac{p_s}{\rho_L RT} = 1 + \delta_L \hat{\Phi}^r_\delta(\delta_L, \tau) \tag{17}$$

$$\frac{p_s}{\rho_V RT} = 1 + \delta_V \hat{\Phi}^r_\delta(\delta_V, \tau) \tag{18}$$

$$\frac{p_s}{RT}\left(\frac{1}{\rho_V} - \frac{1}{\rho_L}\right) - \ln\left(\frac{\rho_L}{\rho_V}\right) = \hat{\Phi}^r(\delta_L, \tau) - \hat{\Phi}^r(\delta_V, \tau) \tag{19}$$

After the structure and coefficients of the classical Helmholtz function were initially optimized, we found the Ginzburg number Gi, the amplitude a_{20} in the kernel term,

and the crossover parameters m_0, v_1 and d_1 in Eq. (11) from a non-linear regression analysis (NRA). For this purpose, we used the algorithm proposed by Levenberg and Marquardt [13]. In the NRA, in addition to the linear experimental data mentioned above, we also use the non-linear $\rho(P, T)$, $C_p(T, p)$, $w(T, p)$ experimental data, as well as the $C_V(\rho, T)$ data generated in the asymptotic critical region for CO_2 with the CREOS-97 program [34]. After the NRA procedure, using the fixed values of the non-linear crossover parameters Gi, a_{20}, m_0 and d_1 we repeat the STW regression for the optimization of the structure of the crossover EOS and linear coefficients a_m. If the resulting structure-optimized crossover EOS satisfies the defined statistical criteria, the optimization is terminated; otherwise another cycle of the NRA with the following STW regression is repeated till the statistical criteria are fully satisfied. In every optimization cycle, each term in the crossover EOS is tested for its statistical significance and intercorrelations; the least significant or statistically irrelevant terms are deleted or replaced by other more representative terms selected from the term-bank. In addition to the polynomial and exponential terms shown in Eq. (2), the term-bank also includes specially designed Guassian terms. These terms were added into the term-bank to improve the representation of different thermodynamic properties along the saturation curve, as discussed by Span and Wagner [15]. Because of the crossover formulation of the GSTW algorithm, the non-analytical functional terms introduced by Span and Wagner [15] were not included in the term-bank. For carbon dioxide, which was chosen in this paper as an example, the term-bank contains 169 functional terms, a bank that is much smaller than that used in the Span and Wagner [15] algorithm. However, as we will show below, even with this restricted term-bank the GSTW algorithm allows us to develop a more compact and more physically correct (in the critical region) EOS than the state-of-the-art EOS developed by Span and Wagner [15].

An essential part of the GSTW regression algorithm described above is a calculation of the statistical weights for the experimental data-points, which are used in the optimization procedure. The overall combination of the optimized weights and careful selection of data points used in the regression determine the optimal EOS to be developed with the GSTW algorithm. In order to eliminate the random scatter in terms of the dependent experimental variable y_n we use here the Guassian error prorogation formula in the form

$$\sigma_{r_n}^2 = \sigma_{y_n}^2 + \sum_{k=1}^{K} \left(\frac{\partial y_n}{\partial x_k} \sigma_{x_k} \right)^2 \tag{20}$$

where $\partial y_n/\partial x_k$ has the effect of transferring the random scatter in the independent variable x_k to the dependent variable y_n. For the calculation of $\partial y_n/\partial x_k$ an EOS obtained in the previous step, or any other accurate EOS developed previously can be used. The variance $\sigma_{x_k}^2$ is estimated from the experimental uncertainties associated with the property measurements. For multi-property regression, relative weighting for a given data type taken from different sources must be used. The final expression for the total weight of a single data-point is given by:

$$W_n = \frac{f_t}{\sigma_{r_n}^2} = \frac{f_t}{\sigma_{y_n}^2 + \sum_{k=1}^{K} ((\partial y_n/\partial x_k)\sigma_{x_k})^2} \tag{21}$$

where W_n is the weight applied to a given data point n, $\sigma_{r_n}^2$ the variance of that data point and f_t is a relative weight of the selected data type given with respect to different data sources which is applied uniformly to all data points from the selected data source. For determination of the optimal values of f_t we used the simplex method proposed by Nelder and Mead [35].

4. Results and discussion

In this work, we have chosen carbon dioxide as an example to demonstrate the utility of the proposed GSTW algorithm. Carbon dioxide is one of the most commonly used solvents in supercritical extraction because its critical point temperature is close to normal atmospheric temperature. The low critical temperature of carbon dioxide makes it possible for various chemical processes to be carried out in the critical or extended critical region. This in turn requires accurate thermodynamic descriptions in the region around the critical point. Since the CO_2 critical point is easily reached in the laboratory, extensive experimental measurements have been made in the critical region for carbon dioxide and the data situation is exceptionally good. From this point of view, carbon dioxide serves as a reference substance for theoretical studies dealing with the critical region of pure fluids. Span and Wagner have published an international standard reference EOS for carbon dioxide in 1996 [15]; therefore, we can also compare our results to this international standard equation. It is important to note that our objective in this study is not to replace the current international standard; rather we are trying to develop a more compact, yet accurate equation of state that is also valid in the critical region.

The selected experimental data set contains $P\rho T$, second virial coefficient, isochoric heat capacity and speed of sound data. Speed of sound data were included into the linear regression procedure only through their corresponding linear forms $(\partial P/\partial \rho)_T$. In addition, data have been calculated from auxiliary equations (independent correlations of saturation properties) in order to be able to apply the Maxwell conditions for vapor–liquid equilibrium (VLE) boundary (e.g., so that we have both saturated densities and the vapor pressure at a given temperature). Span and Wagner [15] give complete lists and critical evaluations of experimental data available for carbon dioxide; thus, for more information, the reader is referred to that paper. The critical point parameters used in this work for carbon dioxide were identical to those used by Span and Wagner, viz., $T_c = 304.1282$ K, $P_c = 7.3773$ MPa and $\rho_c = 467.6$ kg/m^3. The universal gas constant was taken to be 8.31451 J/mol K.

Table 1
Coefficients and exponents of the MCEOS

m	a_m	i_m	j_m	k_m	α_m	β_m	γ_m	ϵ_m
1	$0.381610732 \times 10^{0}$	1	0					
2	$-0.336280780 \times 10^{1}$	1	2					
3	$0.200829312 \times 10^{1}$	1	2.5					
4	$0.454298732 \times 10^{-1}$	2	−.5					
5	$0.228133353 \times 10^{0}$	2	3					
6	$0.119698464 \times 10^{-1}$	4	0					
7	$0.359109876 \times 10^{-4}$	8	0					
8	$-0.222364636 \times 10^{0}$	1	4	1				
9	$-0.193237919 \times 10^{0}$	2	5	1				
10	$-0.823288163 \times 10^{0}$	4	3	1				
11	$0.646314236 \times 10^{-1}$	4	5	1				
12	$-0.184330530 \times 10^{-1}$	6	4	1				
13	$-0.552448222 \times 10^{-1}$	1	5	2				
14	$-0.588413132 \times 10^{-1}$	2	5	2				
15	$0.521870986 \times 10^{-4}$	12	3	2				
16	$0.519231475 \times 10^{0}$	4	2.5	1				
17	$-0.206590513 \times 10^{-1}$	3	16	3				
18	$0.155913678 \times 10^{0}$	5	22	4				
19	$-0.136786172 \times 10^{0}$	5	24	4				
20	$-0.246391224 \times 10^{-1}$	6	16	4				
21	$0.111040145 \times 10^{-1}$	7	24	4				
22	$-0.730952937 \times 10^{-3}$	2	1		25.62	324.2	1.03	1
23	$0.297132390 \times 10^{2}$	2	0		26.01	257.5	1.19	1
24	$-0.133881934 \times 10^{3}$	2	1		24.94	332.6	1.18	1
25	$-0.801505391 \times 10^{6}$	3	3		16.74	308.9	1.23	1
26	$0.813279901 \times 10^{6}$	3	3		16.75	309.1	1.23	1

Table 2
System-dependent crossover parameters of the MC EOS

Parameter	Value
a_{20}	0.1715145×10^{3}
$1/Gi$	0.2237161×10^{3}
d_1	−0.1759147
v_1	0.1204884
m_0	0.7012238
b_0	1.0

A 26-term, structure optimized multiparameter crossover equation of state (MC EOS) has been developed using the GSTW algorithm. The structure of MC EOS is given by:

$$\Phi(\delta, t) = \Phi^{r}(\delta, t) + \Phi^{id}(\delta, t) \tag{22}$$

$$\Phi^{r}(\delta, t) = \sum_{m=1}^{7} a_m \delta^{i_m} t^{j_m} + \sum_{m=8}^{21} a_m \delta^{i_m} t^{j_m} \exp(-\delta^{k_m}) + \sum_{m=22}^{26} a_m \delta^{i_m} t^{j_m} \mathrm{e}^{-\alpha_m(\delta - \epsilon_m)^2 - \beta_m(t-\gamma_m)^2} \tag{23}$$

The ideal part of the dimensionless Helmholtz energy is taken from Span and Wagner's work [15]. The values of the exponents and coefficients in Eq. (23) are given in Table 1. In addition, the MC EOS also contains five crossover parameters, which are listed in Table 2. In Table 3, we give the overall statistical comparison between the MC EOS and the state-of-the-art EOS by Span and Wagner [15]. Detailed comparisons of the MC EOS and the SW EOS [15] with experimental data can be found in Ref. [36]; here, we show only comparisons in some typical thermodynamic states.

The deviations between the experimental saturation properties and the corresponding values calculated from Eq. (22) by using the phase equilibrium condition are essentially identical to those obtained with the SW EOS [15]. Vapor pressure data are represented to within ±0.01%. Saturated liquid and vapor densities are represented within ±0.02% up to ∼303.6 K ($T_r = 0.998$). Approaching the critical point from this value, deviations in density increase for both the SW and MC EOS, but these deviations are still within the experimental uncertainty.

High quality $P\rho T$ data sets for carbon dioxide [37–40] are available in the region with pressures up to 13 MPa and temperatures up to 360 K. Figs. 2 and 3 show that the rep-

Table 3
Statistical comparison between the MC EOS and Span and Wagner's EOS

Property	Number of data	MC EOS, %			Span and Wagner, %		
		AAD[a]	BIAS[b]	RMS[c]	AAD	BIAS	RMS
$P_s(T)$[d]	88	0.001	0.000	0.002	0.012	−0.004	0.012
$\rho_L(T)$[d]	88	0.003	−.002	0.006	0.005	−0.004	0.005
$\rho_V(T)$[d]	88	0.006	0.001	0.013	0.014	−0.007	0.018
$B(T)$	32	0.375	0.212	0.492	0.491	−0.089	0.552
$\rho(p, T)$	3901	0.103	−.023	0.328	0.069	−0.019	0.266
$P(\rho, T)$	3901	0.335	0.059	3.079	0.278	0.072	3.059
$C_V(T, \rho)$	751	3.864	−1.67	4.903	3.360	−0.668	4.418
$C_\alpha(T)$	77	0.513	0.002	0.842	0.556	−0.109	0.891
$C_p(T, p)$[e]	359	1.571	−.348	3.154	1.356	−0.029	2.749
$W(T, p)$[f]	406	0.590	0.120	1.180	0.460	−0.070	0.860
$W_s(T)$[f]	41	0.840	0.270	1.370	0.680	0.190	1.210

[a] AAD: average absolute deviation.
[b] BIAS: average deviation.
[c] RMS: reduced mean square.
[d] Calculated from auxiliary equations in Span and Wagner's work [15].
[e] Used only in non-linear fit.
[f] Linearized data used in linear regression.

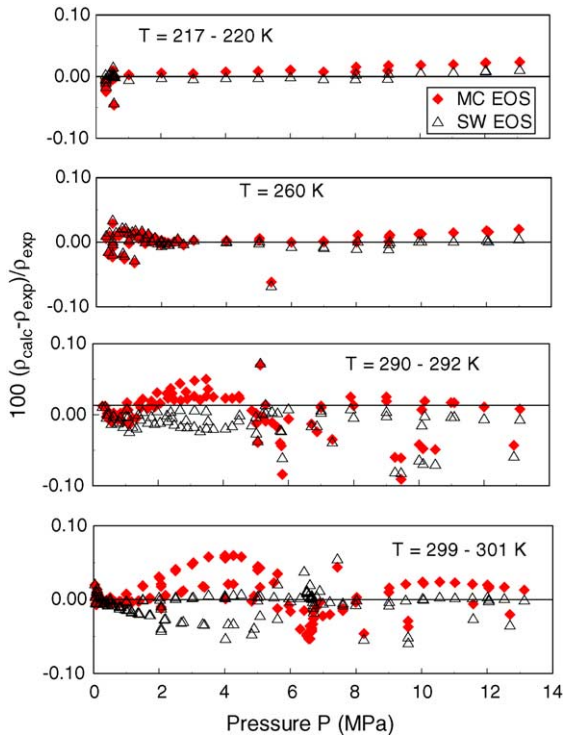

Fig. 2. Relative deviation of accurate data in sub-critical region from values calculated from the MC EOS (solid diamonds). Values calculated from the reference SW are plotted as comparison (upward triangles).

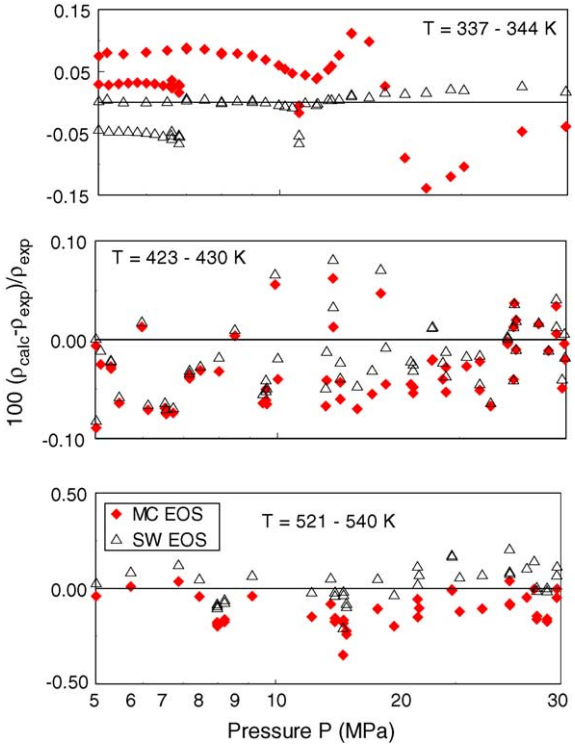

Fig. 4. Relative deviation of accurate data in super-critical region from values calculated from the MC EOS (solid diamonds). Values calculated from the reference SW are plotted as comparison (upward triangles).

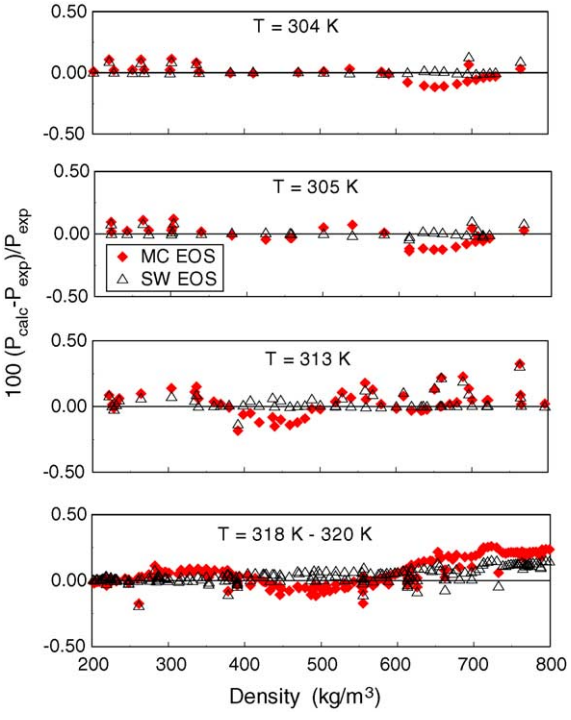

Fig. 3. Relative deviation of accurate data in extended critical region from values calculated from the MC EOS (solid diamonds). Values calculated from the reference SW are plotted as comparison (upward triangles).

resentations of these data by the MC EOS and SW EOS are within their experimental uncertainties. In the extended region where pressures are up to 30 MPa and temperatures are up to 523 K [41,42], the representation of the data by MC EOS is similar to SW EOS except in the region of $337\,K \leq T \leq 344\,K$, as shown in Fig. 4. However, the maximum observed deviation is less than ±0.15% in density.

The deviations between values of the specific isobaric heat capacity calculated from the MC EOS and reliable measurements of C_p [43–46] are given in Fig. 5. The comparison of these data in the gas phase and supercritical regions shows the MC EOS predicts the isobaric heat capacity to within ±0.15%, slightly higher than the experimental uncertainty. Except in the region $T = 363\,K$ and $P > 10$ MPa, the predictions of the MC EOS agree well with those of the SW EOS. As mentioned in the previous section, the caloric behavior of MC EOS is not based on isobaric heat capacity since it is difficult to linearize and include in the linear-least squares regression. The SW EOS is, however, based on precise isobaric heat capacity and speed of sound data. Despite this difference, the MC EOS produces the same accuracy as the SW EOS does for the selected data. Deviations of the specific isochoric heat capacity in gas and liquid phases [47,48] are presented in Fig. 6. As one can see from Fig. 6, the MC EOS shows accuracy similar to the SW EOS along different isochoric curves. As Span and Wagner have pointed out, the large deviations seen in the gas phase are probably due to the uncertainty in the data. At high densities, the data by Magee

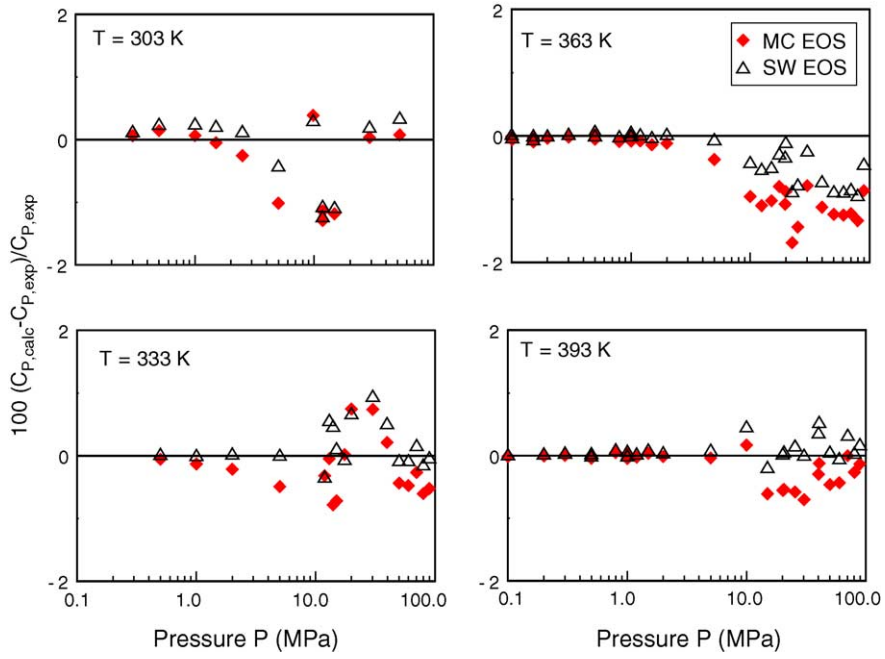

Fig. 5. Relative deviation of selected isobaric heat capacity data from values calculated from the MC EOS (solid diamonds). Values calculated from the reference SW are plotted as comparison (upward triangles).

and Ely [47] are considered as the most reliable results in the liquid state and the MC EOS predicts these data well.

The representation of speed of sound data is a sensitive test of the quality of an EOS for carbon dioxide, especially in the supercritical region and the high-pressure regions. Fig. 7 illustrates the representation of speed of sound data on two representative isotherms from the data set of Novikov and Trelin [49]. The MC EOS gives almost identical predictions as the SW EOS. Prior to this work, the SW EOS was the only EOS, which was capable of reproducing the measurements at 373 K. Not shown in this figure are comparisons with the newer data of Trusler and Estrada-Alexanders [50] that were not available in the development of the SW EOS and were not used in the development of the MC EOS. Comparisons to these data with the MC EOS show an AAD of 0.1% with an RMS deviation of 0.11% for the 61 data points reported.

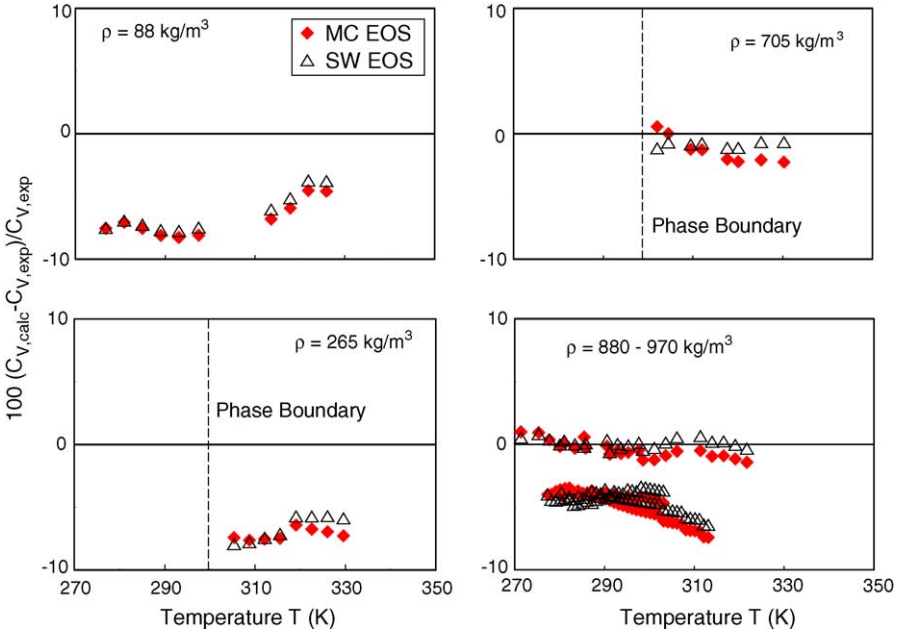

Fig. 6. Relative deviation of selected isochoric heat capacity data from values calculated from the MC EOS (solid diamonds). Values calculated from the reference SW are plotted as comparison (upward triangles).

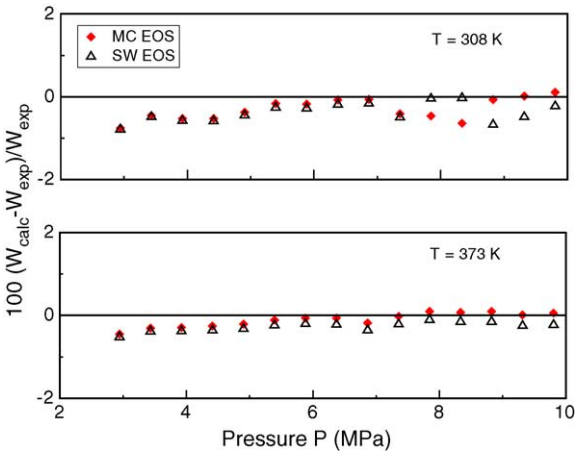

Fig. 7. Relative deviation of speed of sound data in super-critical region from values calculated from the MC EOS (solid diamonds). Values calculated from the reference SW are plotted as comparison (upward triangles).

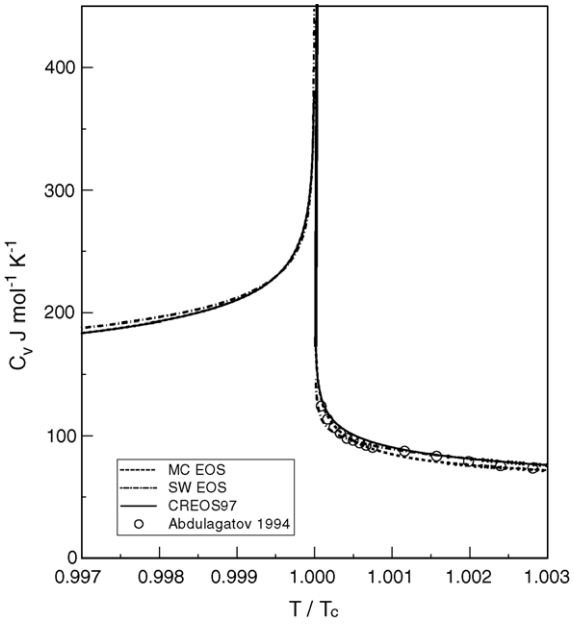

Fig. 9. The isochoric heat capacity of carbon dioxide along the critical isochores as a function of reduced density. The solid curve represents values calculated from the crossover model, the dashed curve corresponds to values calculated from the MC EOS, and the dotted-dashed curve indicates values from the SW EOS. The circles represent experimental values by Abdulagatov et al. [51].

In order to detail the representation of thermodynamic properties in the immediate vicinity of the critical point with the MC and SW EOS, values calculated from a theoretically based crossover model (CREOS97) [34] are included in our comparisons. These data are needed due to the lack of experimental measurements asymptotically close to the critical point. Comparisons between the MC EOS and SW EOS for the isochoric heat capacity and speed of sound along the near-critical isotherm versus reduced density are shown in Fig. 8. As is seen in this figure the SW EOS is unable to describe the divergence of the specific isochoric heat capacity and the speed of sound along the isothermal curve asymptotically close to the critical point (down to dimensionless temperature departure $\tau = 10^{-7}$). However, the MC EOS predicts asymptotic behavior similar to CREOS97. In the regions away from the critical point, all three equations agree in their predictions.

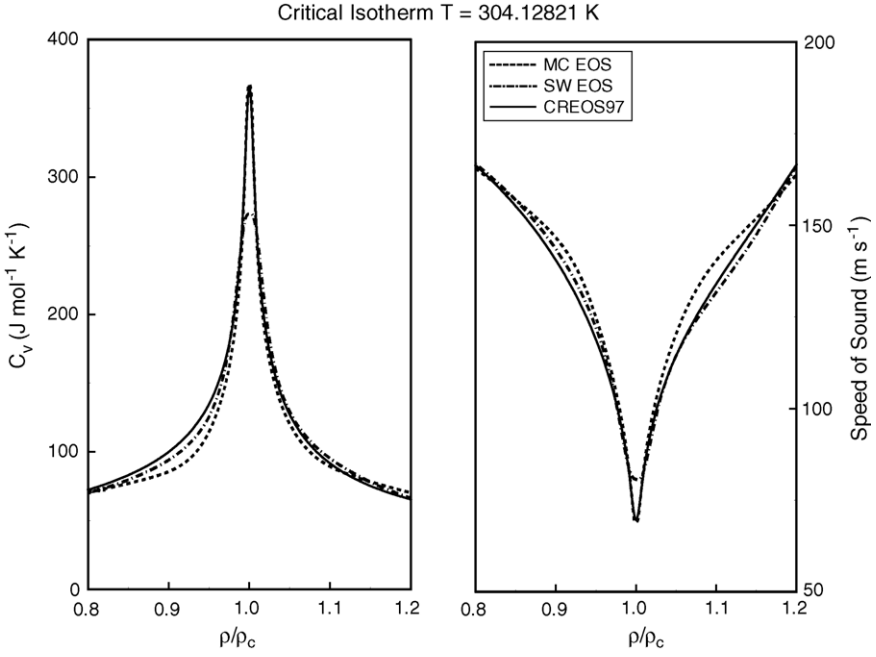

Fig. 8. The isochoric heat capacity and speed of sound of carbon dioxide along near-critical isotherms as a function of reduced density. The solid curve represents values calculated from the crossover model, the dashed curve corresponds to values from the MC EOS, and the dotted-dashed curve indicates values from the SW EOS.

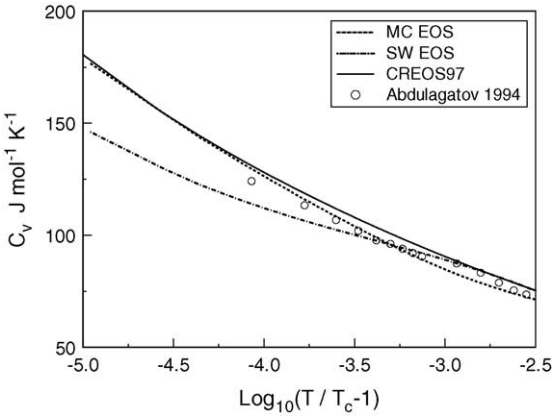

Fig. 10. The isochoric heat capacity of carbon dioxide along the critical isochore as a function of reduced density. The solid curve represents values calculated from the crossover model, the dashed curve corresponds to values calculated from the MC EOS, and the dotted-dashed curve indicates values from SW EOS. The circles represent experimental values by Abdulagatov et al. [51].

We also have compared the MC EOS and SW EOS along the critical isochore below and above the critical point with the results being shown in Figs. 9 and 10. Clearly, the three equations give identical results along the critical isochore below the critical point. However, the situation is different when comparisons are made along the critical isochore above the critical point as shown in the right half of Figs. 9 and 10. Asymptotically close to the critical point (in the region $1.0005 \leq T/T_c \leq 1.003$), the MC EOS and CREOS97 give the same behavior for the isochoric heat capacity while the SW EOS does not follow the trend. Away from the critical point, the SW EOS rejoins the CREOS97 curve but the MC EOS shows some departure. The experimental measurements by Abdulagatov et al. [51] shown in Figs. 9 and 10 were included during the development of the MC EOS, however, they were not available when SW EOS and CREOS97 were developed. Therefore, the MC EOS follows the data trend of these experimental measurements while the other two models do not.

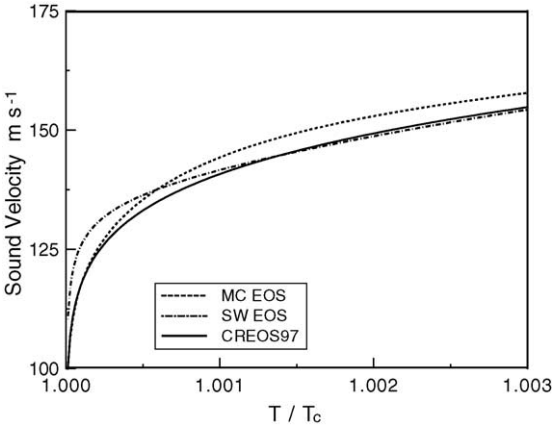

Fig. 11. The speed of sound of carbon dioxide along the critical isochore as a function of reduced density. The solid curve represents values calculated from the crossover model, the dashed curve corresponds to values calculated from MC EOS, and the dotted-dashed curve indicates values calculated from SW EOS.

In Fig. 11, the asymptotic behavior of speed of sound in the vicinity of the critical point is shown. The MC EOS gives the same asymptotic behavior (infinitely small) of the speed of sound as CREOS97, while SW EOS shows some deviations asymptotically close to the critical point. The departure of MC EOS from CREOS97 and SW EOS away from the critical point can also be explained by the addition of experimental measurements by Abdulagatov et al. [51] that were not available when the first two EOS models were fit.

5. Conclusions

Empirical multiparameter equations of state obtained from experimental data sets by the means of linear or non-linear regression allow accurate description for the thermodynamic properties over a wide-range of states. However, these equations cannot predict the correct asymptotic behavior in the vicinity of the critical point. Therefore, non-analytical terms need to be added to the EOS during the regression to overcome this shortcoming. Several examples of this type of EOS have already been developed for carbon dioxide, nitrogen and water, etc. Even though these equations improve the description of the thermal and caloric properties close to the critical point, they fail to describe the asymptotic behaviors for the specific isochoric heat capacity in the immediate vicinity of the critical point. Furthermore, the non-analytical terms used are usually substance specific and cannot be transferred to other fluid systems directly, i.e., the parameters used (including the exponents) have to be redefined.

Incorporation of the crossover formulation into the equation of state gives an accurate description of the asymptotic behavior in the immediate vicinity of the critical point. Since the crossover formulation obeys universal scaling laws, it is applicable to different fluid systems. In the previous work of Kiselev and Friend [22], it has been shown that the crossover EOS improves the description in the critical region while retaining the same accuracy in regions away from the critical point. Once given the appropriate crossover parameters, the crossover EOS could be easily applied to different systems with high accuracy.

The selection and optimization algorithm proposed in this paper enables the incorporation of the crossover formulation into a multiparameter equation of state. Because of the correct behavior given by the crossover part and the optimized weights for the experimental data points, the intercorrelations in the terms in the EOS are reduced and it is possible to develop a compact but accurate crossover EOS from an optimization procedure based on stepwise regression.

A MC EOS for carbon dioxide was developed by applying the proposed algorithm. There were only 26 terms in the MC EOS, more compact than the reference EOS by Span and

Wagner [15]. In a wide-range of states away from the critical point, the MC EOS shows agreement with the reference EOS for the description of thermodynamic properties. However, in the immediate vicinity of the critical point, the advantages of the crossover EOS are clear, especially in its description of the caloric properties.

The goal of this work was not to develop a new state-of-the-art EOS for the thermodynamic surface for carbon dioxide; rather it was focused on the development of optimization algorithm with a crossover formulation included. We realize that the difference between the MC EOS and SP EOS appears only extremely close to the critical point ($0 < |\tau| \leq 10^{-4}$) where no experimental data are available. Out of this critical region (at $|\tau| > 10^{-4}$), both equations are practically equivalent. Therefore, for practical engineering calculations one can use either of these two equations. Further research will be carried out on the application of the new algorithm proposed in this paper to other fluids of engineering interest.

List of symbols

a_m	coefficients of the crossover equation of state
a_{20}	coefficient of the kernel term
A	Helmholtz energy per mole
C_p	specific isobaric heat capacity
C_V	specific isochoric heat capacity
Gi	Ginzburg number
i	exponents of equation of state
j	exponents of equation of state
k	exponents of equation of state
K	kernel term
m_0, d_1, v_1	crossover parameters
M	molecular weight, length of equation of state
P	pressure
q	argument of crossover function
R	molar gas constant
S	entropy
T	temperature
t	dimensionless temperature
V	volume
W	speed of sound
Y	crossover function
Z	compressibility

Greek letters

α	critical exponent
β	critical exponent
δ	dimensionless density
γ	critical exponent, exponent of equation of state
ε	exponent of equation of state
σ	saturation
μ_0	analytical function of temperature
τ	dimensionless temperature difference
ρ	density
Φ	dimensionless Helmholtz energy
Δ	difference
Δ_1	critical exponent
η	order parameter
$\Delta\Phi$	critical part of dimensionless Helmholtz energy
$\hat{\Phi}^r$	crossover form of the residual Helmholtz energy

Superscripts

id	ideal gas part
r	residual part

Subscripts

0	reference state
c	critical
L	liquid
s	saturation
tri	triple-point
V	vapor

Acknowledgements

The authors are grateful to Prof. Dr. Roland Span of Universität Paderborn, Germany, for providing the program and experimental data for comparisons during the course of this research and for his very useful suggestions in the revision of this manuscript. The authors would like to thank the Department of Energy, Office of Basic Energy Sciences, for the financial support under Grant No. DE-FG03-95ER14568.

Appendix A. Equation of state derivatives

See Tables A.1–A.5 .

Table A.1
Thermodynamic properties in the form of the dimensionless Helmholtz energy $\Phi(\delta, t)$

Property	Dimensionless functional form
Pressure, $P(\rho, T)$	$\frac{P(\rho,T)}{\rho RT} = 1 + \delta\Phi^r_\delta$
Second virial coefficient, $B(T)$	$\rho_c B(T) = \lim_{\delta\to 0}(\Phi^r_\delta)$
Isochoric heat capacity, $C_V(\rho, T)$	$\frac{C_V(\rho,T)}{R} = -t^2(\Phi^{id}_{tt} + \Phi^r_{tt})$
Isobaric heat capacity, $C_p(\rho, T)$	$\frac{C_p}{R} = \frac{C_V}{R} + \frac{(1+\delta\Phi^r_\delta - \delta t\Phi^r_{\delta t})^2}{(1+2\delta\Phi^r_\delta + \delta^2\Phi^r_{\delta\delta})}$

Table A.1 (*Continued*)

Property	Dimensionless functional form
Speed of sound, $u(P, T)$	$\frac{u^2(P,T)}{RT/M_W} = \frac{C_p(P,T)}{C_V(\rho,T)}(1 + 2\delta\Phi^r_\delta + \delta^2\Phi^r_{\delta\delta})$
Enthalpy, $H(\rho, T)$	$\frac{H(\rho,T)}{RT} = 1 + t\Phi^{id}_t + t\Phi^r_t + \delta\Phi^r_\delta$
Gibbs free energy, $G(\rho, T)$	$\frac{G(\rho,T)}{RT} = 1 + \Phi^{id} + \Phi^r - \delta\Phi^r_\delta$
Entropy, $S(\rho, T)$	$\frac{S(\rho,T)}{R} = -(\Phi^{id} + \Phi^r - t\Phi^{id}_t - t\Phi^r_t)$
Internal energy, $U(\rho, T)$	$\frac{U(\rho,T)}{RT} = t(\Phi^{id}_t + \Phi^r_t)$
Derivative of pressure, $\left(\frac{\partial P}{\partial \rho}\right)_T$	$\left(\frac{\partial P}{\partial \rho}\right)_T = RT(1 + 2\delta\Phi^r_\delta + \delta^2\Phi^r_{\delta\delta})$
Derivative of pressure, $\left(\frac{\partial P}{\partial T}\right)_\rho$	$\left(\frac{\partial P}{\partial T}\right)_\rho = R\rho(1 + \delta\Phi^r_\delta - \delta t\Phi^r_{\delta t})$
Fugacity coefficient, $\ln[\varphi(P, T)] = \int_0^P \left[\frac{1}{\rho RT} - \frac{1}{P}\right] dP$	$\ln\varphi = \Phi^r + \delta\Phi^r_\delta - \ln(1 + \delta\Phi^r_\delta)$
Joule–Thomson coefficient, $\mu(P, T) = (\partial T/\partial P)_h$	$\mu R\rho = \frac{-(\delta\Phi^r_\delta + \delta^2\Phi^r_{\delta\delta} + \delta t\Phi^r_{\delta t})}{(1+\delta\Phi^r_\delta - \delta t\Phi^r_{\delta t})^2 - t^2(\Phi^{id}_{tt} + \Phi^r_{tt})(1 + 2\delta\Phi^r_\delta + \delta^2\Phi^r_{\delta\delta})}$

Subscripts denote derivatives with respect to the indicated variable.

Table A.2
Derivatives with respect to δ and t of the polynomial and exponential terms in the residual part of Helmholtz energy

Derivative	Expression
Φ^r_{Pol}	$\sum_{m=1}^{M_1} a_m \delta^{i_m} t^{j_m}$
$\Phi^r_{Pol,\delta}$	$\left(\frac{\partial\Phi^r_{Pol}}{\partial\delta}\right)_t = \sum_{m=1}^{M_1} a_m i_m \delta^{i_m-1} t^{j_m}$
$\Phi^r_{Pol,\delta\delta}$	$\left(\frac{\partial^2\Phi^r_{Pol}}{\partial\delta^2}\right)_t = \sum_{m=1}^{M_1} a_m i_m (i_m - 1)\delta^{i_m-2} t^{j_m}$
$\Phi^r_{Pol,\delta\delta\delta}$	$\left(\frac{\partial^3\Phi^r_{Pol}}{\partial\delta^3}\right)_t = \sum_{m=1}^{M_1} a_m i_m (i_m - 1)(i_m - 2)\delta^{i_m-3} t^{j_m}$
$\Phi^r_{Pol,t}$	$\left(\frac{\partial\Phi^r_{Pol}}{\partial t}\right)_\delta = \sum_{m=1}^{M_1} a_m j_m \delta^{i_m} t^{j_m-1}$
$\Phi^r_{Pol,tt}$	$\left(\frac{\partial^2\Phi^r_{Pol}}{\partial t^2}\right)_\delta = \sum_{m=1}^{M_1} a_m j_m (j_m - 1)\delta^{i_m} t^{j_m-2}$
$\Phi^r_{Pol,\delta t}$	$\left(\frac{\partial^2\Phi^r_{Pol}}{\partial\delta\partial t}\right) = \sum_{m=1}^{M_1} a_m i_m j_m \delta^{i_m-1} t^{j_m-1}$
$\Phi^r_{Pol,\delta tt}$	$\left(\frac{\partial^3\Phi^r_{Pol}}{\partial\delta\partial t^2}\right) = \sum_{m=1}^{M_1} a_m i_m j_m (j_m - 1)\delta^{i_m-1} t^{j_m-2}$
Φ^r_{Exp}	$\sum_{m=M_1+1}^{M_2} a_m \delta^{i_m} t^{j_m} \exp(-\gamma_m \delta^{k_m})$
$\Phi^r_{Exp,\delta}$	$\left(\frac{\partial\Phi^r_{Exp}}{\partial\delta}\right)_t = \sum_{m=M_1+1}^{M_2} a_m \delta^{i_m-1}(i_m - \gamma_m k_m \delta^{k_m}) t^{j_m} \exp(-\gamma_m \delta^{k_m})$
$\Phi^r_{Exp,\delta\delta}$	$\left(\frac{\partial^2\Phi^r_{Exp}}{\partial\delta^2}\right)_t = \sum_{m=M_1+1}^{M_2} a_m \delta^{i_m-2}[(i_m - \gamma_m k_m \delta^{k_m})(i_m - 1 - \gamma_m k_m \delta^{k_m}) - (\gamma_m k_m)^2 \delta^{k_m}] t^{j_m} \exp(-\gamma_m \delta^{k_m})$
$\Phi^r_{Exp,\delta\delta\delta}$	$\left(\frac{\partial^3\Phi^r_{Exp}}{\partial\delta^3}\right)_t = \sum_{m=M_1+1}^{M_2} a_m \delta^{i_m-3} t^{j_m} \exp(-\gamma_m \delta^{k_m}) \left\{ \begin{array}{l} (i_m - 3 - \gamma_m k_m \delta^{k_m})[(i_m - \gamma_m k_m \delta^{k_m})(i_m - 1 - \gamma_m k_m \delta^{k_m}) - (\gamma_m k_m)^2 \delta^{k_m}] \\ +[i_m - 1 - \gamma_m k_m \delta^{k_m} - 2(\gamma_m k_m)^2 \delta^{k_m}](i_m - \gamma_m k_m \delta^{k_m}) - k_m(\gamma_m k_m)^2 \delta^{k_m} \end{array} \right\}$

Table A.2 (*Continued*)

Derivative	Expression
$\Phi^{\mathrm{r}}_{\mathrm{Exp},t}$	$\left(\frac{\partial\Phi^{\mathrm{r}}_{\mathrm{Exp}}}{\partial t}\right)_{\delta} = \sum_{m=M_1+1}^{M_2} a_m j_m \delta^{i_m} t^{j_m-1} \exp(-\gamma_m \delta^{k_m})$
$\Phi^{\mathrm{r}}_{\mathrm{Exp},tt}$	$\left(\frac{\partial^2\Phi^{\mathrm{r}}_{\mathrm{Exp}}}{\partial t^2}\right)_{\delta} = \sum_{m=M_1+1}^{M_2} a_m j_m (j_m-1) \delta^{i_m} t^{j_m-2} \exp(-\gamma_m \delta^{k_m})$
$\Phi^{\mathrm{r}}_{\mathrm{Exp},\delta t}$	$\left(\frac{\partial^2\Phi^{\mathrm{r}}_{\mathrm{Exp}}}{\partial\delta\partial t}\right) = \sum_{m=M_1+1}^{M_2} a_m j_m \delta^{i_m-1} (i_m - \gamma_m k_m \delta^{k_m}) t^{j_m-1} \exp(-\gamma_m \delta^{k_m})$
$\Phi^{\mathrm{r}}_{\mathrm{Exp},\delta tt}$	$\left(\frac{\partial^3\Phi^{\mathrm{r}}_{\mathrm{Exp}}}{\partial\delta\partial t^2}\right) = \sum_{m=M_1+1}^{M_2} a_m j_m (j_m-1) \delta^{i_m-1} (i_m - \gamma_m k_m \delta^{k_m}) t^{j_m-2} \exp(-\gamma_m \delta^{k_m})$

Table A.3
Derivatives with respect to δ and t of Gaussian terms in the residual part of Helmholtz energy

Abbreviation	Derivatives
$\Phi^{\mathrm{r}}_{\mathrm{GS}}$	$\sum_{m=M_2+1}^{M_3} a_m t^{i_m} \delta^{j_m} \mathrm{e}^{-\alpha_m(\delta-\in_m)^2-\beta_m(t-\gamma_m)^2}$
$\Phi^{\mathrm{r}}_{\mathrm{GS},\delta}$	$\left(\frac{\partial\Phi^{\mathrm{r}}_{\mathrm{GS}}}{\partial\delta}\right)_t = \sum_{m=M_2+1}^{M_3} a_m t^{i_m} \delta^{j_m} \mathrm{e}^{-\alpha_m(\delta-\in_m)^2-\beta_m(t-\gamma_m)^2} \left[\frac{j_m}{\delta} - 2\alpha_m(\delta-\in_m)\right]$
$\Phi^{\mathrm{r}}_{\mathrm{GS},\delta\delta}$	$\left(\frac{\partial^2\Phi^{\mathrm{r}}_{\mathrm{GS}}}{\partial\delta^2}\right)_t = \sum_{m=M_2+1}^{M_3} a_m t^{i_m} \delta^{j_m} \mathrm{e}^{-\alpha_m(\delta-\in_m)^2-\beta_m(t-\gamma_m)^2} \cdot \left[\left(\frac{j_m}{\delta} - 2\alpha_m(\delta-\in_m)\right)^2 - \frac{j_m}{\delta^2} - 2\alpha_m\right]$
$\Phi^{\mathrm{r}}_{\mathrm{GS},\delta\delta\delta}$	$\left(\frac{\partial^3\Phi^{\mathrm{r}}_{\mathrm{GS}}}{\partial\delta^3}\right)_t = \sum_{m=M_2+1}^{M_3} a_m t^{i_m} \delta^{j_m} \mathrm{e}^{-\alpha_m(\delta-\in_m)^2-\beta_m(t-\gamma_m)^2} \cdot \left\{\begin{array}{l}\left[\left(\frac{j_m}{\delta} - 2\alpha_m(\delta-\in_m)\right)^2 - \frac{j_m}{\delta^2} - 2\alpha_m\right]\left[\frac{j_m}{\delta} - 2\alpha_m(\delta-\in_m)\right] \\ +2\left(\frac{j_m}{\delta} - 2\alpha_m(\delta-\in_m)\right)\left(-\frac{j_m}{\delta^2} - 2\alpha_m\right) + 2\frac{j_m}{\delta^3}\end{array}\right\}$
$\Phi^{\mathrm{r}}_{\mathrm{GS},t}$	$\left(\frac{\partial\Phi^{\mathrm{r}}_{\mathrm{GS}}}{\partial t}\right)_{\delta} = \sum_{m=M_2+1}^{M_3} a_m t^{i_m} \delta^{j_m} \mathrm{e}^{-\alpha_m(\delta-\in_m)^2-\beta_m(t-\gamma_m)^2} \left[\frac{i_m}{t} - 2\beta_m(t-\gamma_m)\right]$
$\Phi^{\mathrm{r}}_{\mathrm{GS},tt}$	$\left(\frac{\partial^2\Phi^{\mathrm{r}}_{\mathrm{GS}}}{\partial t^2}\right)_{\delta} = \sum_{m=M_2+1}^{M_3} a_m t^{i_m} \delta^{j_m} \mathrm{e}^{-\alpha_m(\delta-\in_m)^2-\beta_m(t-\gamma_m)^2} \cdot \left[\left(\frac{i_m}{t} - 2\beta_m(t-\gamma_m)\right)^2 - \frac{i_m}{t^2} - 2\beta_m\right]$
$\Phi^{\mathrm{r}}_{\mathrm{GS},\delta t}$	$\left(\frac{\partial^2\Phi^{\mathrm{r}}_{\mathrm{GS}}}{\partial\delta\partial t}\right) = \sum_{m=M_2+1}^{M_3} a_m t^{i_m} \delta^{j_m} \mathrm{e}^{-\alpha_m(\delta-\in_m)^2-\beta_m(t-\gamma_m)^2} \cdot \left[\frac{j_m}{\delta} - 2\alpha_m(\delta-\in_m)\right]\left[\frac{i_m}{t} - 2\beta_m(t-\gamma_m)\right]$
$\Phi^{\mathrm{r}}_{\mathrm{GS},\delta tt}$	$\left(\frac{\partial^3\Phi^{\mathrm{r}}_{\mathrm{GS}}}{\partial\delta\partial t^2}\right) = \sum_{m=M_2+1}^{M_3} a_m t^{i_m} \delta^{j_m} \mathrm{e}^{-\alpha_m(\delta-\in_m)^2-\beta_m(t-\gamma_m)^2} \cdot \left[\frac{j_m}{\delta} - 2\alpha_m(\delta-\in_m)\right]\left[\left(\frac{i_m}{t} - 2\beta_m(t-\gamma_m)\right)^2 - \frac{i_m}{t^2} - 2\beta_m\right]$

Table A.4
Thermophysical properties in terms of the crossover dimensionless residual Helmholtz energy $\hat{\Phi}^{\mathrm{r}}(\delta, t)$

Property	Dimensionless functional form
Enthalpy	$\frac{h(\rho,T)}{RT} = 1 + t\Phi^{\mathrm{id}}_t + t\hat{\Phi}^{\mathrm{r}}_t + \delta\hat{\Phi}^{\mathrm{r}}_{\delta}$
Gibbs free energy	$\frac{g(\rho,T)}{RT} = 1 + \Phi^{\mathrm{id}} + \hat{\Phi}^{\mathrm{r}} - \delta\hat{\Phi}^{\mathrm{r}}_{\delta}$
Pressure	$\frac{p(\rho,T)}{\rho RT} = 1 + \delta\hat{\Phi}^{\mathrm{r}}_{\delta}$
Entropy	$\frac{s(\rho,T)}{R} = -(\Phi^{\mathrm{id}} + \hat{\Phi}^{\mathrm{r}} - t\Phi^{\mathrm{id}}_t - t\hat{\Phi}^{\mathrm{r}}_t)$
Internal energy	$\frac{u(\rho,T)}{RT} = t(\Phi^{\mathrm{id}}_t + \hat{\Phi}^{\mathrm{r}}_t)$
Isochoric heat capacity	$\frac{C_V(\rho,T)}{R} = -t^2(\Phi^{\mathrm{id}}_{tt} + \hat{\Phi}^{\mathrm{r}}_{tt})$

Table A.4 (*Continued*)

Property	Dimensionless functional form
Isobaric heat capacity	$\frac{C_p}{R} = \frac{C_V}{R} + \frac{(1+\delta\hat{\Phi}^r_\delta - \delta t\hat{\Phi}^r_{\delta t})^2}{(1+2\delta\hat{\Phi}^r_\delta + \delta^2\hat{\Phi}^r_{\delta\delta})}$
Second virial coefficient	$\rho_c b(T) = \rho_c \lim_{\delta\to 0}\left(\frac{\delta\hat{\Phi}^r_\delta}{\rho}\right)$
Speed of sound	$\frac{w^2(\rho,T)}{RT/M} = \frac{C_p(\rho,T)}{C_V(\rho,T)}(1 + 2\delta\hat{\Phi}^r_\delta + \delta^2\hat{\Phi}^r_{\delta\delta})$

Table A.5
Derivatives of the dimensionless crossover Helmholtz energy

$$\left(\frac{\partial\hat{\Phi}^r}{\partial\delta}\right)_t = \frac{d\hat{\Phi}^r}{d\delta} + \left(\frac{\partial\hat{\Phi}^r}{\partial\delta}\right)_{\bar{t},t}\left(\frac{\partial\bar{\delta}}{\partial\delta}\right)_t + \left(\frac{\partial\hat{\Phi}^r}{\partial t}\right)_{\bar{\delta},t}\left(\frac{\partial\bar{t}}{\partial\delta}\right)_t + \left(\frac{\partial[-K(\tau)]}{\partial\delta}\right)_t$$

$$\left(\frac{\partial\hat{\Phi}^r}{\partial t}\right)_\delta = \frac{d\hat{\Phi}^r}{dt} + \left(\frac{\partial\hat{\Phi}^r}{\partial t}\right)_{\bar{\delta},\delta}\left(\frac{\partial\bar{t}}{\partial t}\right)_\delta + \left(\frac{\partial\hat{\Phi}^r}{\partial\delta}\right)_{\bar{t},\delta}\left(\frac{\partial\bar{\delta}}{\partial t}\right)_\delta + \left(\frac{\partial[-K(\tau)]}{\partial t}\right)_\delta$$

$$\left(\frac{\partial^2\hat{\Phi}^r}{\partial\delta^2}\right)_t = \frac{d^2\hat{\Phi}^r}{d\delta^2} + \left(\frac{\partial\hat{\Phi}^r}{\partial\delta}\right)_{\bar{t},t}\left(\frac{\partial^2\bar{\delta}}{\partial\delta^2}\right)_t + \left(\frac{\partial^2\hat{\Phi}^r}{\partial\delta^2}\right)_{\bar{t},t}\left(\frac{\partial\bar{\delta}}{\partial\delta}\right)_t^2 + \left(\frac{\partial^2\hat{\Phi}^r}{\partial\delta t}\right)\left(\frac{\partial\bar{\delta}}{\partial\delta}\right)_t\left(\frac{\partial\bar{t}}{\partial\delta}\right)_t + \left(\frac{\partial^2\hat{\Phi}^r}{\partial\delta t}\right)\left(\frac{\partial\bar{t}}{\partial\delta}\right)_t\left(\frac{\partial\bar{\delta}}{\partial\delta}\right)_t + \left(\frac{\partial\hat{\Phi}^r}{\partial t}\right)_{\bar{\delta},t}\left(\frac{\partial^2\bar{t}}{\partial\delta^2}\right)_t + \left(\frac{\partial^2\hat{\Phi}^r}{\partial t^2}\right)_{\bar{\delta},t}\left(\frac{\partial\bar{t}}{\partial\delta}\right)_t^2 + \left(\frac{\partial^2[-K(\tau)]}{\partial\delta^2}\right)_t$$

$$\left(\frac{\partial^2\hat{\Phi}^r}{\partial t^2}\right)_\delta = \frac{d^2\hat{\Phi}^r}{dt^2} + \left(\frac{\partial^2\hat{\Phi}^r}{\partial t^2}\right)_{\bar{\delta},\delta}\left(\frac{\partial\bar{t}}{\partial t}\right)_\delta^2 + \left(\frac{\partial\hat{\Phi}^r}{\partial t}\right)_{\bar{\delta},\delta}\left(\frac{\partial^2\bar{t}}{\partial t^2}\right)_\delta + \left(\frac{\partial^2\hat{\Phi}^r}{\partial t\delta}\right)\left(\frac{\partial\bar{t}}{\partial t}\right)_\delta\left(\frac{\partial\bar{\delta}}{\partial t}\right)_\delta + \left(\frac{\partial^2\hat{\Phi}^r}{\partial\delta t}\right)\left(\frac{\partial\bar{\delta}}{\partial t}\right)_\delta\left(\frac{\partial\bar{t}}{\partial t}\right)_\delta + \left(\frac{\partial^2\hat{\Phi}^r}{\partial\delta^2}\right)_{\bar{t},\delta}\left(\frac{\partial\bar{\delta}}{\partial t}\right)_\delta^2 + \left(\frac{\partial\hat{\Phi}^r}{\partial\delta}\right)_{\bar{t},\delta}\left(\frac{\partial^2\bar{\delta}}{\partial t^2}\right)_\delta + \left(\frac{\partial^2[-K(\tau)]}{\partial t^2}\right)_\delta$$

$$\left(\frac{\partial^2\hat{\Phi}^r}{\partial\delta\partial t}\right) = \frac{d^2\hat{\Phi}^r}{d\delta dt} + \left(\frac{\partial\hat{\Phi}^r}{\partial\delta}\right)_{\bar{t}}\left(\frac{\partial^2\bar{\delta}}{\partial\delta\partial t}\right) + \left(\frac{\partial^2\hat{\Phi}^r}{\partial\delta^2}\right)_{\bar{t}}\left(\frac{\partial\bar{\delta}}{\partial\delta}\right)_t\left(\frac{\partial\bar{\delta}}{\partial t}\right)_\delta + \left(\frac{\partial^2\hat{\Phi}^r}{\partial\delta t}\right)\left(\frac{\partial\bar{\delta}}{\partial\delta}\right)_t\left(\frac{\partial\bar{t}}{\partial t}\right)_\delta + \left(\frac{\partial^2\hat{\Phi}^r}{\partial\delta t}\right)\left(\frac{\partial\bar{t}}{\partial\delta}\right)_t\left(\frac{\partial\bar{\delta}}{\partial t}\right)_\delta + \left(\frac{\partial\hat{\Phi}^r}{\partial t}\right)_{\bar{\delta}}\left(\frac{\partial^2\bar{t}}{\partial\delta\partial t}\right) + \left(\frac{\partial^2\hat{\Phi}^r}{\partial t^2}\right)_{\bar{\delta}}\left(\frac{\partial\bar{t}}{\partial\delta}\right)_t\left(\frac{\partial\bar{t}}{\partial t}\right)_\delta + \left(\frac{\partial^2[-K(\tau)]}{\partial\delta\partial t}\right)_t$$

$$\frac{d\hat{\Phi}^r}{d\delta} = -\frac{1}{\delta} + \frac{P_0(t)}{\delta^2}$$

$$\frac{d^2\hat{\Phi}^r}{d\delta^2} = \frac{1}{\delta^2} - \frac{2P_0(t)}{\delta^3}$$

$$\frac{d\hat{\Phi}^r}{dt} = \left(\frac{d\Phi^r(1,t)}{dt}\right) - \eta\frac{dP_0(t)}{dt}$$

$$\frac{d^2\hat{\Phi}^r}{dt^2} = \left(\frac{d^2\Phi^r(1,t)}{dt^2}\right) - \eta\frac{d^2P_0(t)}{dt^2}$$

$$\frac{d^2\hat{\Phi}^r}{d\delta dt} = \frac{1}{\delta^2}\frac{dP_0(t)}{dt}$$

$$\left(\frac{\partial\hat{\Phi}^r}{\partial\delta}\right)_{\bar{t},t} = \left(\frac{\partial\Phi^r}{\partial\delta}\right)_{\bar{t},t} + \frac{1}{\delta} - \frac{1}{\delta^2}P_0(\bar{t})$$

$$\left(\frac{\partial\hat{\Phi}^r}{\partial t}\right)_{\bar{\delta},t} = \left(\frac{\partial\Phi^r(\bar{t},\bar{\delta})}{\partial t}\right)_{\bar{\delta},t} - \left(\frac{\partial\Phi^r(\bar{t},1)}{\partial t}\right)_{\bar{\delta},t} + \bar{\eta}\frac{dP_0(\bar{t})}{dt}$$

$$\left(\frac{\partial^2\hat{\Phi}^r}{\partial\delta^2}\right)_{\bar{t},t} = \left(\frac{\partial^2\Phi^r}{\partial\delta^2}\right)_{\bar{t},t} - \frac{1}{\delta^2} + \frac{2}{\delta^3}P_0(\bar{t})$$

$$\left(\frac{\partial^2\hat{\Phi}^r}{\partial\bar{t}^2}\right)_{\bar{\delta},t} = \left(\frac{\partial^2\Phi^r(\bar{t},\bar{\delta})}{\partial\bar{t}^2}\right)_{\bar{\delta},t} - \left(\frac{\partial^2\Phi^r(\bar{t},1)}{\partial\bar{t}^2}\right)_{\bar{\delta},t} + \bar{\eta}\frac{d^2P_0(\bar{t})}{d\bar{t}^2}$$

$$\left(\frac{\partial^2\hat{\Phi}^r}{\partial\delta\bar{t}}\right)_t = \left(\frac{\partial^2\Phi^r(\bar{t},\bar{\delta})}{\partial\bar{t}\delta}\right)_t - \frac{1}{\delta^2}\frac{dP_0(\bar{t})}{dt}$$

$$\left(\frac{\partial\bar{\delta}}{\partial\delta}\right)_t = \left(\frac{\bar{\delta}}{\delta}\right)^2\left(\frac{\partial\bar{\eta}}{\partial\eta}\right)_t$$

$$\left(\frac{\partial\bar{\delta}}{\partial\bar{t}}\right)_\delta = \left(\frac{\bar{\delta}}{\bar{t}}\right)^2\left(\frac{\partial\bar{\eta}}{\partial\tau}\right)_\delta$$

$$\left(\frac{\partial\bar{t}}{\partial\delta}\right)_t = \left(\frac{\bar{t}}{\delta}\right)^2\left(\frac{\partial\bar{\tau}}{\partial\eta}\right)_t$$

$$\left(\frac{\partial\bar{t}}{\partial t}\right)_\delta = \left(\frac{\bar{t}}{t}\right)^2\left(\frac{\partial\bar{\tau}}{\partial\tau}\right)_\delta$$

Table A.5 (*Continued*)

$$\left(\frac{\partial^2\bar{\delta}}{\partial\delta^2}\right)_t = -2\left[\frac{(\partial\bar{\delta}/\partial\delta)_t}{\delta}\right] + 2\left[\frac{(\partial\bar{\delta}/\partial\delta)_t^2}{\delta}\right] - \left(\frac{\bar{\delta}^2}{\delta^4}\right)\left(\frac{\partial^2\bar{\eta}}{\partial\eta^2}\right)_t$$

$$\left(\frac{\partial^2\bar{\delta}}{\partial t^2}\right) = 2\left(\frac{\bar{\delta}}{t}\right)^2\left(\frac{\partial\bar{\eta}}{\partial\tau}\right)_\delta\left[\frac{1}{\delta}\frac{\partial\bar{\delta}}{\partial t} - \frac{1}{t}\right] - \frac{1}{t^2}\left(\frac{\bar{\delta}}{t}\right)^2\left(\frac{\partial^2\bar{\eta}}{\partial\tau^2}\right)_\delta$$

$$\left(\frac{\partial^2\bar{\delta}}{\partial\delta\partial t}\right) = \frac{2}{\delta}\left(\frac{\partial\bar{\delta}}{\partial\delta}\right)\left(\frac{\partial\bar{\delta}}{\partial t}\right) - \left(\frac{\bar{\delta}}{\delta t}\right)^2\left(\frac{\partial^2\bar{\eta}}{\partial\eta\partial\tau}\right)$$

$$\left(\frac{\partial^2\bar{t}}{\partial\delta^2}\right)_t = \frac{2}{t}\left(\frac{\partial\bar{t}}{\partial\delta}\right)_t^2 - 2\left(\frac{\partial\bar{t}/\partial\delta}{\delta}\right)_t - \frac{\bar{t}^2}{\delta^4}\left(\frac{\partial^2\bar{\tau}}{\partial\eta^2}\right)_t$$

$$\left(\frac{\partial^2\bar{t}}{\partial t^2}\right)_\delta = 2\left(\frac{\bar{t}}{t}\right)^2\left(\frac{\partial\bar{\tau}}{\partial\tau}\right)_\delta\left[\left(\frac{\partial\bar{t}}{\partial t}\right)\frac{1}{t} - \frac{1}{t}\right] - \frac{1}{t^2}\left(\frac{\bar{t}}{t}\right)^2\left(\frac{\partial^2\bar{\tau}}{\partial\tau^2}\right)_\delta$$

$$\left(\frac{\partial^2\bar{t}}{\partial\delta\partial t}\right) = \frac{2}{t}\left(\frac{\partial\bar{t}}{\partial\delta}\right)\left(\frac{\partial\bar{t}}{\partial t}\right) - \left(\frac{\bar{t}}{\delta t}\right)^2\left(\frac{\partial^2\bar{\tau}}{\partial\eta\partial\tau}\right)$$

$$\frac{\mathrm{d}\bar{\eta}}{\mathrm{d}\delta} = -\frac{1}{\delta^2} = -(\bar{\eta}+1)^2$$

$$\frac{\partial^2\varphi}{\partial\delta^2} = \frac{2}{\delta^3}$$

$$\frac{\mathrm{d}\eta}{\mathrm{d}\delta} = -\frac{1}{\delta^2}$$

$$\frac{\partial^2\varphi}{\partial\delta^2} = \frac{2}{\delta^3}$$

$$\frac{\mathrm{d}\eta}{\mathrm{d}\delta} = -\frac{1}{\delta^2}$$

References

[1] R.T. Jacobsen, S.G. Penoncello, E.W. Lemmon, R. Span, in: J.V. Sengers, C.J. Peters, H.J. White Jr. (Eds.), Equations of State for Fluids and Fluid Mixtures. Part II, Elsevier, Amsterdam, 2000, pp. 844–879.
[2] R. Span, Multiparameter Equations of State—An Accurate Source of Thermodynamic Property Data, Springer-Verlag, Berlin, 2000.
[3] W. Wagner, AIChE Annual Meeting, Reno, 2001.
[4] W. Wagner, Fortschr. -Ber. VDI-Z. 3 (1974) 39.
[5] K.M. de Reuck, B. Armstrong, Cryogenics 25 (1979) 505.
[6] R. Schmit, W. Wagner, Fluid Phase Equilib. 19 (1985) 175.
[7] U. Setzmann, W. Wagner, Int. J. Thermophys. 10 (1989) 1103.
[8] J. Ewers, W. Wagner, in: J.V. Sengers (Ed.), Proceedings of the Eighth Symposium on Thermophysical Properties, vol. I. Thermophysical Properties of Fluids, ASME, New York, 1982, p. 78.
[9] U. Setzmann, W. Wagner, J. Phys. Chem. Ref. Data 20 (1991) 1061.
[10] K.B. Shubert, Application of linear regression decision algorithms in the development of equations of state for refrigerants R134a and R123, M.S. Thesis, Department of Chemical Engineering and Petroleum Refining, Colorado School of Mines, Golden, 1994, p. 247.
[11] K.B. Shubert, J.F. Ely, Int. J. Thermophys. 16 (1995) 101.
[12] J. Ahrendts, H.D. Baehr, Int. Chem. Eng. 21 (1981) 557.
[13] J. Ahrendts, H.D. Baehr, Int. Chem. Eng. 21 (1981) 572.
[14] C. Tegeler, R. Span, W. Wagner, J. Phys. Chem. Ref. Data 28 (1999) 779.
[15] R. Span, W. Wagner, J. Phys. Chem. Ref. Data 25 (1996) 1509.
[16] W. Wagner, A. Pruss, J. Phys. Chem. Ref. Data 31 (2002) 387.
[17] R. Span, E.W. Lemmon, R.T. Jacobsen, W. Wagner, A. Yokozeki, J. Phys. Chem. Ref. Data 29 (2000) 1361.
[18] J. Smukala, R. Span, W. Wagner, J. Phys. Chem. Ref. Data 29 (2000) 1053.
[19] R. Span, W. Wagner, E.W. Lemmon, R.T. Jacobson, Fluid Phase Equilib. 183–184 (2001) 1.
[20] J.V. Sengers, J.M.H.L. Sengers, Annu. Rev. Phys. Chem. 37 (1986) 189.
[21] M.A. Anisimov, S.B. Kiselev, Sov. Tech. Rev. B Therm. Phys., vol. 3, Harwood Academic, Chur-Melbourne, 1992.
[22] S.B. Kiselev, D.G. Friend, Fluid Phase Equilib. 155 (1999) 33.
[23] S.B. Kiselev, Fluid Phase Equilib. 147 (1998) 7.
[24] S.B. Kiselev, D.G. Friend, Fluid Phase Equilib. 162 (1999) 51.
[25] S.B. Kiselev, J.F. Ely, J. Chem. Phys. 119 (2003) 8645.
[26] S.B. Kiselev, J.F. Ely, Ind. Eng. Chem. Res. 38 (1999) 4993.
[27] S.B. Kiselev, J.F. Ely, Fluid Phase Equilib. 174 (2000) 93.
[28] S.B. Kiselev, J.F. Ely, I.M. Abdulagatov, J.W. Magee, Int. J. Thermophys. 21 (2000) 1373.
[29] C. McCabe, S.B. Kiselev, Fluid Phase Equilib. 219 (2004) 3.
[30] S.B. Kiselev, J.F. Ely, L. Lue, J.R. Elliott, Fluid Phase Equilib. 200 (2002) 121.
[31] A.Z. Patashinskii, V.L. Pokrovskii, Fluctuation Theory of Phase Transitions, Pergamon, New York, 1979.
[32] Z.Y. Chen, P.C. Albright, J.V. Sengers, Phys. Rev. A 41 (1990) 3161.
[33] R.D. McCarty, Determination of thermodynamic properties from the experimental p-V-T relationships, in: B. Le Neindre, B. Vodar, (Eds.), Experimental Thermodynamics, Vol. II-Experimental Thermodynamics of Non-Reacting Fluids, Butterworth, Ltd., London, England, 1975, 501–526.
[34] S.B. Kiselev, Fluid Phase Equilib. 128 (1997) 1.
[35] J.A. Nelder, R. Mead, Comput. J. 7 (1965) 308.
[36] L. Sun, Development of advanced equations of state for engineering application, Ph.D. Thesis, Chemical Engineering, Colorado School of Mines, Golden, USA, 2003.
[37] W. Duschek, R. Kleinrahm, W. Wagner, J. Chem. Thermodyn. 22 (1990) 827.
[38] X.Y. Guo, R. Kleinrahm, W. Wagner, Lehrsstuhl fur Thermodunamik, Ruhr-Universitat-Bochum, Germany, Bochum, 1992.
[39] R. Gilgen, R. Kleinrahm, W. Wagner, J. Chem. Thermodyn. 24 (1992) 1493.
[40] P. Nowak, T. Tielks, R. Kleinrahm, W. Wagner, J. Chem. Thermodyn. 29 (1997) 885.

[41] J. Klimeck, R. Kleinrahm, W. Wagner, J. Chem. Thermodyn. 33 (2001) 251.
[42] K. Brachthauser, R. Kleinrahm, W. Wagner, VDI Fortschritt-Ber., Reihe 8, Nr. 371, VDI-Verlag, Dusseldorf, 1993.
[43] J.F. Masi, B. Petkof, J. Res. Natl. Bur. Stand. 48 (1952) 179.
[44] R. Bender, K. Bier, G. Maurer, Ber. Bunsenges. Phys. Chem. 85 (1981) 778.
[45] G. Ernst, G. Maurer, E. Wiederuh, J. Chem. Thermodyn. 21 (1989) 53.
[46] G. Ernst, U.E. Hochberg, J. Chem. Thermodyn. 21 (1989) 407.
[47] J.W. Magee, J.F. Ely, Int. J. Thermophys. 7 (1986) 1163.
[48] K.I. Amirkhanov, N.G. Polikhronidi, Teploenergetica 18 (1971) 59.
[49] I.I. Novikov, Y.S. Trelin, Teploenergetica 9 (1962) 79.
[50] A.F. Estrada-Alexanders, J.P.M. Trusler, J. Chem. Thermodyn. 30 (1998) 1589.
[51] I.M. Abdulagatov, N.G. Polikhronidi, R.G. Batyrova, Ber. Bunsenges. Phys. Chem. 98 (1994) 1068.